

Identification of chirality of chiral multifold fermions in anti-crystals

Yan Sun,^{1,*} Qiunan Xu,¹ Yang Zhang,² Congcong Le,¹ and Claudia Felser^{1,3}

¹*Max Planck Institute for Chemical Physics of Solids, 01187 Dresden, Germany*

²*Department of Physics, Massachusetts Institute of Technology, Cambridge, Massachusetts 02139, USA*

³*Center for Nanoscale Systems, Faculty of Arts and Sciences, Harvard University, 11 Oxford Street, LISE 308 Cambridge, Massachusetts 02138, USA*

The chirality of chiral multifold fermions in reciprocal space is related to the chirality of the crystal lattice structure in real space. In this work, we propose a strategy to detect and identify opposite-chirality multifold fermions in nonmagnetic systems by means of second-order optical transports. The chiral crystals are related by an inversion operation and cannot overlap with each other by any experimental operation, and the chiral multifold fermions in the crystals host opposite chiralities for a given k -point. A change of chirality is indicated by a sign change of the second-order charge current dominated by chiral fermions. This strategy is effective to study the relationship between chiralities in reciprocal and real spaces by utilizing bulk transport.

Multifold massless fermions with nonzero topological charge are attracting increasing attention in the field of topological materials. In contrast to four-fold degenerate Dirac and doubly degenerate Weyl fermions, which have directly analogous fundamental particles in high-energy physics, multifold fermions do not follow the Poincaré symmetry in high-energy physics; rather, they follow the crystal symmetry and, therefore, do not have counterparts among real particles. [1, 2]. More interestingly, the multifold fermions in chiral crystals can host nonzero topological charges with a Chern number greater than 1, which results in both nontrivial topological surface states and exotic bulk transport properties.

Since multifold fermions are located at high-symmetry points, they guarantee long surface Fermi arcs spanning the entire Brillouin zone (BZ) [3–6]. In addition to the huge separation of opposite topological charges in momentum space, the absence of mirror symmetry leads to their large separation in energy space, providing an ideal platform for the study of the quantized circular photogalvanic effect (CPGE) [3, 5, 7, 8]. Soon after theoretical prediction, the long Fermi arcs, high-order degenerated band crossings, and quantized CPGE were observed in the predicted chiral crystals by ARPES [9–13] and optical measurements [14].

Recently, via ARPES measurements, a sign change of the Fermi velocity of surface Fermi arcs was observed in semimetals having chiral multifold fermions and crystals of opposite chiralities, implying a deep relationship between the chiral lattices in real space and the chiral fermions in momentum space [13]. This relationship offers a new degree of freedom to tune the chiral fermions and corresponding physical properties. Hence, it is important to understand the relationship of chirality between real and reciprocal spaces as well as the resulting phenomena. In the present study, based on a symmetry analysis and numerical calculations, we provide a strategy for detecting the interplay between chiral fermions

and chiral crystals from the transport perspective. Since the crystal structures of the same compound with opposite chiralities are related by an inversion operation, the relationship between chiral fermions and chiral crystals can be detected by means of nonlinear optical and electrical transports.

Here, we focus on materials in the space group $P2_13$ because, to date, all the experimentally verified materials with chiral multifold fermions belong to this space group. For a crystal with the space group $P2_13$, owing to the glide two-fold rotation symmetry ($s_{2x} = \{c_{2x} | (\frac{1}{2} \frac{1}{2} 0)\}$, $s_{2y} = \{c_{2y} | (0 \frac{1}{2} \frac{1}{2})\}$, and $s_{2z} = \{c_{2z} | (\frac{1}{2} 0 \frac{1}{2})\}$), corresponding glide mirror operations can be obtained through a simple inversion operation. Therefore, chiral crystals with opposites chiralities in the space group $P2_13$ are connected by a simple inversion operation, as shown in Fig. 1(a,b). In any other crystal structure without c_2 or glide c_2 rotation symmetry, a mirror operation can be also equivalent to an inversion operation in combination with an experimental c_2 rotation operation because samples can be rotated by any angle in experiments.

In compounds with the space group $P2_13$, the chiral multifold fermions located at Γ and R have four-fold and six-fold degeneracy, respectively [1–6]. Similar to Weyl fermions, these two types of chiral multifold fermions can be described in a unified form using the Hamiltonian $H = \chi \vec{k} \cdot \vec{S}$, with $\chi = \pm 1$ [2] and the pseudospin matrix following $[S_i, S_j] = i\epsilon_{ijk} S_k$. The four-fold degeneracy at Γ points is a spin-3/2 excitation with a 4×4 pseudospin matrix, and the topological charge has a Chern number of ± 4 when the two lower bands are occupied. The six-fold degeneracy at the R point is constructed by double spin-1 Weyl fermions and a doubly degenerate quadratic band; hence, the 3×3 pseudospin matrix can be used to describe this six-fold degeneracy, as shown in Fig. 1(e). Since the spin-1 Weyl fermions have a Chern number of ± 2 , the corresponding topological charge for double spin-1 Weyl fermions is ± 4 , making the whole system follow a “no-go theorem.” For both spin-1 and spin-3/2 excitation, the sign of the topological charge is dependent on the sign of the prefactor χ . Under an inversion op-

* ysun@cpfs.mpg.de

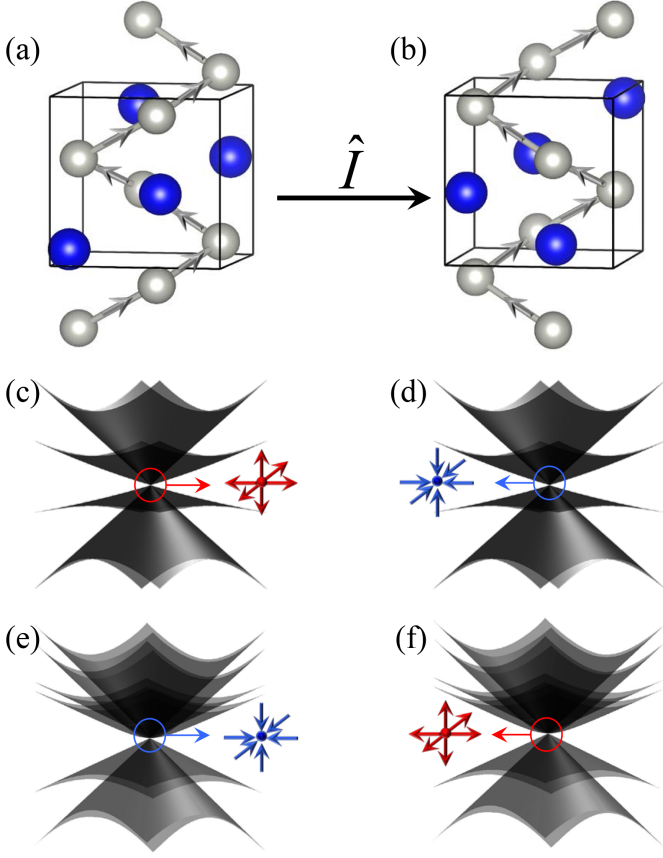


FIG. 1. Inversion of chirality in a chiral crystal structure leads to the inversion of chirality for chiral multifold fermions. (a, b) Crystal lattice structures with opposite chiralities of semimetals in the space group P213 with chiral multifold fermions, taking RhSi as an example. (c, d) Four-fold degenerate fermion with spin-3/2 excitation at the Γ point. (e, f) Double three-fold degenerate fermions with spin-1 excitation at the R point. The local effective Hamiltonians around crossing points are $H = -\vec{k} \cdot \vec{S}_{4 \times 4}$, $H = \vec{k} \cdot \vec{S}_{4 \times 4}$, $H = -\vec{k} \cdot \vec{S}_{3 \times 3}$, and $H = \vec{k} \cdot \vec{S}_{3 \times 3}$ for (c-f), respectively.

eration, $H(\vec{k})$ is changed to $H(-\vec{k})$. While keeping the form of energy dispersion, chirality changes the sign, as is evident from a comparison of Fig. 1 (c-f).

Though the chirality of a multifold fermion is reversed by the inversion operation, time-reversal symmetry makes the net Berry phase zero in the entire BZ. Therefore, the anomalous Hall effect cannot be used to probe the change of chirality. However, the second-order responses are odd with respect to inversion, which provides the possibility to detect the change in chirality of multifold fermions of semimetals in anti-crystals.

There are mainly two types of transports based on second-order responses: nonlinear optical effects and the nonlinear Hall effect from Berry curvature dipole [15–19]. The specific crystal symmetry makes the off-diagonal elements of the nonlinear Hall conductivity tensor zero, and only one independent diagonal element is allowed.

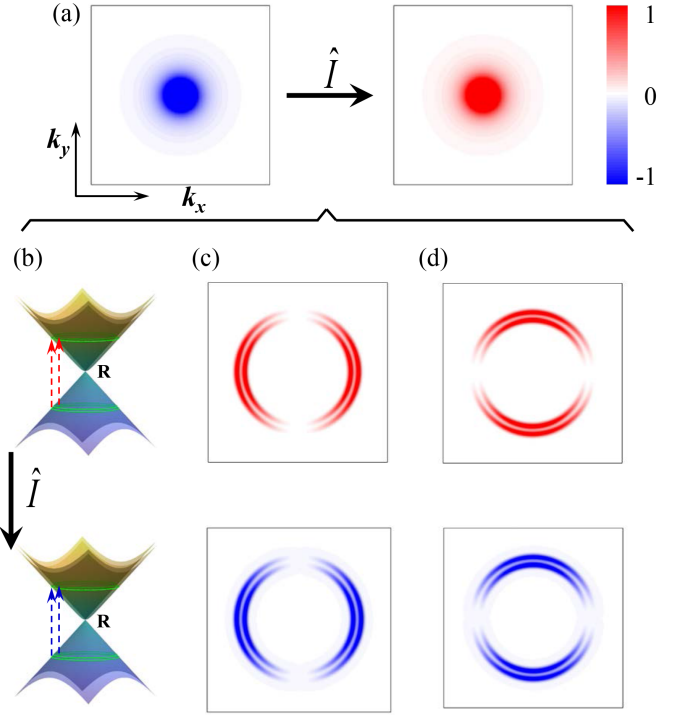


FIG. 2. (a) Inversion-operation-induced sign change for local Berry curvature (Ω_z) distribution around multifold chiral fermions. (b) Schematic of light excitation between the lower and upper cones of multifold fermions. The green rings represent the transition path for a given frequency. The light excitation from the hot ring-like distribution for (c) $\tilde{\chi}_{yz}^{CPGE,x}(\vec{k}; 0, \omega, -\omega)$ and (d) $\tilde{\chi}_{yz}^{LPGE,x}(\vec{k}; 0, \omega, -\omega)$. $\tilde{\chi}_{yz}^{CPGE,x}$ and $\tilde{\chi}_{yz}^{LPGE,x}$ change the sign with the inversion operation on the crystal structure. The plot is in the $k_z = \pi$ plane around the R point. The color bars are in arbitrary units.

However, owing to time-reversal symmetry,

$$\begin{aligned}
 & \int f_0 (D_{xx} + D_{yy} + D_{zz}) d\vec{k} \\
 &= \int f_0 \left(\frac{\partial \Omega_x}{\partial k_x} + \frac{\partial \Omega_y}{\partial k_y} + \frac{\partial \Omega_z}{\partial k_z} \right) d\vec{k} \\
 &= \int \Omega_x \frac{\partial f_0}{\partial k_x} + \Omega_y \frac{\partial f_0}{\partial k_y} + \Omega_z \frac{\partial f_0}{\partial k_z} d\vec{k} \\
 &= \int \vec{\Omega} \frac{\partial f_0}{\partial \vec{k}} d\vec{k} \\
 &= \int \vec{\Omega} \delta(E - E_F) d\vec{k} \\
 &= 0
 \end{aligned} \tag{1}$$

makes the trace of Berry curvature dipole zero; consequently, nonlinear Hall effects from Berry curvature

dipole vanish in materials belonging to the space group $P2_13$. Therefore, we will take the second-order optical transports, CPGE and the linear photogalvanic effect (LPGE), to investigate responses to the reversal of chirality of multifold fermions.

In crystals without an inversion center, polarized light can generate a photocurrent in the material [15–17, 20–28]. In contrast to the photovoltaic effect in p-n junctions, the photovoltaic effect induced by polarized light is dependent only on the bulk band structure and not limited by the band gap. Therefore, the polarized-light-induced photoelectric effect is also called the bulk photovoltaic effect (BPVE). Depending on the polarization of incident light, the photocurrent can be classified into two types: an injection current induced by circularly polarized light $\frac{d\vec{j}_a}{dt} = \chi_{bc}^{C,a}(0, \omega, -\omega)E_b(\omega)E_c(-\omega)$ and a shift current induced by linearly polarized light $\vec{j}_a = \chi_{bc}^{L,a}(0, \omega, -\omega)E_b(\omega)E_c(-\omega)$ [17], where $E_{i(j,k)}(\omega)$ is the electrical field with $i, j, k = x, y, z$.

First, we check the response of the local k -space distribution of these two nonlinear optical conductivities to the inversion of chirality. The CPGE tensor is purely imaginary and can be written as [17]

$$\chi_{bc}^{C,a}(0, \omega, -\omega) = \frac{e^3 \pi}{\hbar V} \sum_{\vec{k}} \sum_{m,n} f_{nm}^{\vec{k}} \Delta_{\vec{k},mn}^a [r_{\vec{k},mn}^c, r_{\vec{k},nm}^b] \delta(\hbar\omega - E_{\vec{k},mn}), \quad (2)$$

and the LPGE tensor is real and can be written as [17]

$$\chi_{bc}^{L,a}(0, \omega, -\omega) = \frac{ie^3 \pi}{\hbar V} \sum_{\vec{k}} \sum_{m,n} f_{nm}^{\vec{k}} (r_{\vec{k},mn}^b r_{\vec{k},nm}^{c;a} + r_{\vec{k},mn}^c r_{\vec{k},nm}^{b;a}) \delta(\hbar\omega - E_{\vec{k},mn}), \quad (3)$$

with

$$r_{\vec{k},nm}^a = \frac{v_{\vec{k},nm}^a}{i\omega_{\vec{k},nm}} \quad (4)$$

and

$$r_{\vec{k},nm}^{a;b} = \frac{i}{\omega_{\vec{k},nm}} [v_{\vec{k},nm}^a \Delta_{\vec{k},nm}^a + v_{\vec{k},nm}^b \Delta_{\vec{k},nm}^b - \omega_{\vec{k},nm}^{ab}] + \sum_{p \neq n,m} \left(\frac{v_{\vec{k},np}^a v_{\vec{k},pm}^b}{\omega_{\vec{k},pm}} - \frac{v_{\vec{k},np}^b v_{\vec{k},pm}^a}{\omega_{\vec{k},np}} \right), \quad (5)$$

where $f_{\vec{k},nm}^{\vec{k}} = f_n^{\vec{k}} - f_m^{\vec{k}}$ is the difference of the Fermi-Dirac distribution between two bands, $E_{\vec{k},mn} = E_{\vec{k},n} - E_{\vec{k},m}$ is the energy difference between the bands, $v_{\vec{k},nm}^a = \frac{1}{\hbar} \langle n | \partial_a \hat{H} | m \rangle$ is the velocity matrix, $\Delta_{\vec{k},nm}^a = v_{\vec{k},nn}^a - v_{\vec{k},mm}^a$ is the Fermi velocity difference between the bands, and $\omega_{\vec{k},nm}^{ab} = \frac{1}{\hbar^2} \langle n(\vec{k}) | \partial_{ab}^2 H | m(\vec{k}) \rangle$. For the convenience of analysis of the microscopic relationship between

the band structure and second-order conductivity, we set

$$\tilde{\chi}_{bc}^{C,a}(\vec{k}; 0, \omega, -\omega) = \sum_{m,n} f_{nm}^{\vec{k}} \Delta_{\vec{k},mn}^a [r_{\vec{k},mn}^c, r_{\vec{k},nm}^b] \delta(\hbar\omega - E_{\vec{k},mn}) \quad (6)$$

and

$$\tilde{\chi}_{bc}^{L,a}(\vec{k}; 0, \omega, -\omega) = \sum_{m,n} f_{nm}^{\vec{k}} (r_{\vec{k},mn}^b r_{\vec{k},nm}^{c;a} + r_{\vec{k},mn}^c r_{\vec{k},nm}^{b;a}) \delta(\hbar\omega - E_{\vec{k},mn}). \quad (7)$$

For the second-order response, $\vec{j}_a = \chi_{bc}^a E_b E_c$, the sign of the conductivity χ will become negative on inverting each of the coordinate indices. For the specific space group $P2_13$, the glide c_2 rotation symmetry s_{2z} changes the sign of the optical conductivity tensor with the z -index appearing an even number of times, making them zero. Similarly, when the x - or y -index appears an even number of times, the elements with the index vanish because of s_{2x} or s_{2y} , respectively. Furthermore, owing to the D_2 subgroup, the three indexes yield the same optical conductivity, and only one nonzero independent tensor element of each index remains for both second-order CPGE and LPGE: $\chi_{yz}^{C(L),x} = \chi_{zx}^{C(L),y} = \chi_{xy}^{C(L),z}$. Thus, taking the six-fold degeneracy at the R point as an example, we analyze the changes of distribution functions of $\tilde{\chi}_{yz}^{C(L),x}(\vec{k}; 0, \omega, -\omega)$ with respect to the inversion operation.

As discussed above, the chirality of the chiral fermions change the sign of counterpart crystal structures with opposite chirality. Accordingly, since the chiral fermions are Berry curvature monopoles, the Berry curvatures at a given k -point around the six-fold degenerate points are also opposite in two lattice crystal structures with inverted chiralities, as shown in in Fig. 2(a) for Ω_z .

The chirality of the Berry curvature is also related to the correlation between the band structure and polarized light. As shown in Fig. 2(b) and (c), when the Fermi level is at the linear crossing point, two transitions exist for a selected transition energy in the $k_z = 0$ plan. These two transitions form two hot rings for both distribution functions, $\tilde{\chi}_{yz}^{C,x}(\vec{k}; 0, \omega, -\omega)$ and $\tilde{\chi}_{yz}^{L,x}(\vec{k}; 0, \omega, -\omega)$, as shown in the upper panels of Fig. 2(c) and (d). The positions of the hot rings remain the same after the inversion operation, but their signs switch, as shown in the bottom panels of Fig. 2(c) and (d).

To check the second-order optical conductivity, the distribution functions must be integrated over the entire BZ. By employing the Hamiltonian of the tight-binding model [3], we calculated the second-order conductivity tensor, which fully is consistent with the symmetry constrained tensor shapes. Owing to the large separation of the opposite-chirality fermions in energy space, the trace of CPGE is a quantized value in units $i\pi \frac{e^3}{\hbar^2}$. In Fig. 3(a), we show the transition-energy-dependent CPGE for $\chi_{yz}^{C,x}$, corresponding to β_{xx} in Ref. [8]. Since we only take one

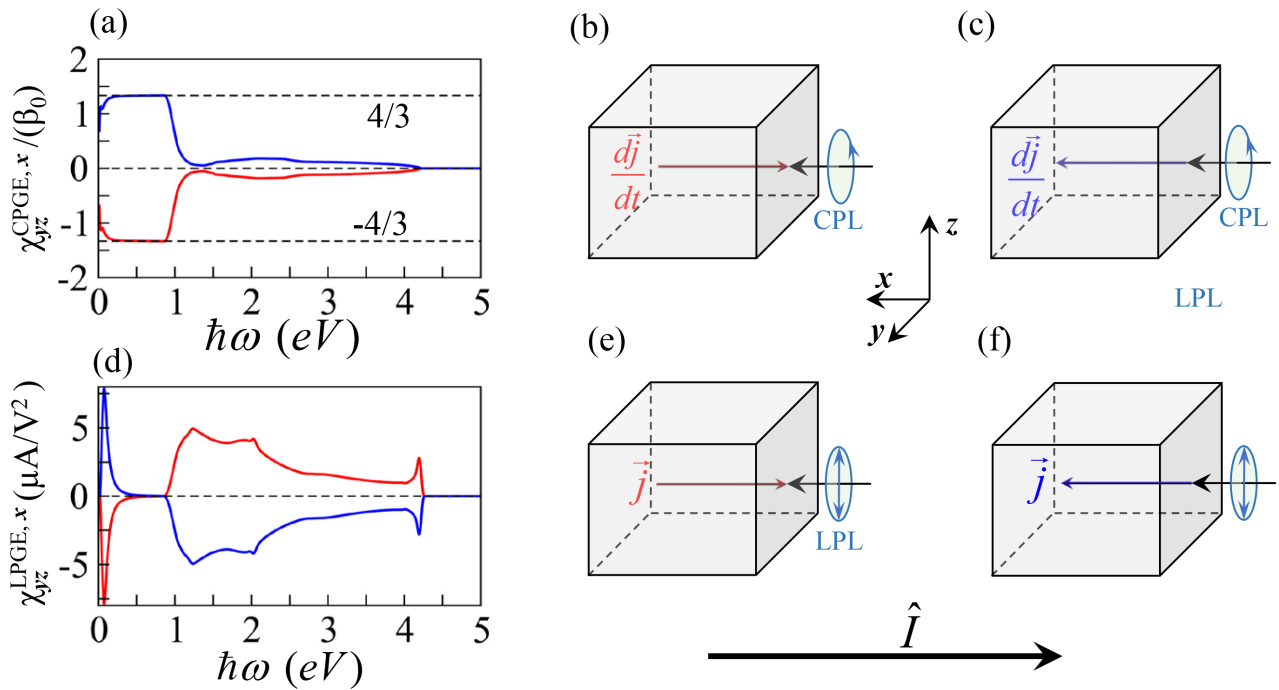


FIG. 3. Frequency-dependent second-order conductivity for (a) CPGE and (d)LPGE. The red and blue curves correspond to opposite chiralities of the chiral fermions. The signs of all three conductivities change with the switch of chirality of the crystal structure. Schematic of the experimental setup for identifying multifold fermions in anti-crystals by (b, c) CPGE and (e, f) LPGE. CPL in (b, c) represents circularly polarized light, and LPL in (e, f) represents linearly polarized light. The calculations were performed using the tight-binding model reported in Ref. [3] with the parameters $v_1 = 1.0$, $v_p = -1.0$, $v_{r1} = 0.0$, $v_{r2} = -0.01$, $v_{r3} = 0.01$, $v_{s1} = -0.01$, $v_{s2} = 0.0$, and $v_{s3} = 0$ and an onsite term $v_0 = 0.01$ to shift the degeneracy at the R point to the Fermi level. $\beta_0 = i\pi \frac{e^3}{\hbar^2}$ in (a).

component of the trace term, a third of the quantized value exists in the range of ~ 0.1 to ~ 0.8 eV. On inverting the crystal structure to its counterpart with opposite chirality, the sign of CPGE changes. Therefore, for circularly polarized light with a specific helix, the generated voltage drop is opposite for the same type of chiral fermions with left- and right-handed chirality.

We present a schematic setup for the experimental measurement of $\chi_{yz}^{C,x}$ as an example. On applying circularly polarized light along the x direction, with its electrical field locked in the $y - z$ plane, an injection current along $-x$ is generated. When using the same circularly polarized light along the same direction for the same compound with opposite chirality, the sign of the injection current changes, as shown in Fig. 3(b) and (c). Though the LPGE is not quantized, a strong shift current is expected in this class of chiral crystals because of the strong inversion-symmetry breaking [29]. By applying linearly polarized light in the same direction, a shift current along x is generated, and a sign change occurs for its anti-crystal, as shown in Fig. 3(d-f). The sign change of the strong signal of shift current can be easily detected.

In summary, the switch of chirality of chiral multifold fermions is related to the sign change of charge currents generated by second-order electrical and optical responses. This relationship provides an effective bulk-transport approach to experimentally identify the chirality of chiral fermions of the same type, as well as the relationship between the chirality of chiral fermions in reciprocal space and the crystal structure in real space.

ACKNOWLEDGMENTS

Thanks to Inti Sodemann for the helpful discussion. This work was financially supported by the ERC Advanced Grant No. 291472 ‘Idea Heusler’, ERC Advanced Grant No. 742068 ‘TOPMAT’. This work was performed in part at the Center for Nanoscale Systems (CNS), a member of the National Nanotechnology Coordinated Infrastructure Network (NNCI), which is supported by the National Science Foundation under NSF award no. 1541959. CNS is part of Harvard University. Some of our calculations were carried out on the Cobra cluster of MPCDF, Max Planck society.

- [1] J. L. Manes, “Existence of bulk chiral fermions and crystal symmetry,” *Physical Review B*, vol. 85, no. 15, p. 155118, 2012.
- [2] B. Bradlyn, J. Cano, Z. Wang, M. Vergniory, C. Felser, R. Cava, and B. A. Bernevig, “Beyond Dirac and Weyl fermions: Unconventional quasiparticles in conventional crystals,” *Science*, vol. 353, no. 6299, p. aaf5037, 2016.
- [3] G. Chang, S.-Y. Xu, B. J. Wieder, D. S. Sanchez, S.-M. Huang, I. Belopolski, T.-R. Chang, S. Zhang, A. Bansil, H. Lin, *et al.*, “Unconventional Chiral Fermions and Large Topological Fermi Arcs in RhSi,” *Phy. Rev. Lett.*, vol. 119, no. 20, p. 206401, 2017.
- [4] P. Tang, Q. Zhou, and S.-C. Zhang, “Multiple types of topological fermions in transition metal silicides,” *Phy. Rev. Lett.*, vol. 119, no. 20, p. 206402, 2017.
- [5] G. Chang, B. J. Wieder, F. Schindler, D. S. Sanchez, I. Belopolski, S.-M. Huang, B. Singh, D. Wu, T.-R. Chang, T. Neupert, *et al.*, “Topological quantum properties of chiral crystals,” *Nature materials*, vol. 17, no. 11, p. 978, 2018.
- [6] T. Zhang, Z. Song, A. Alexandradinata, H. Weng, C. Fang, L. Lu, and Z. Fang, “Double-weyl phonons in transition-metal monosilicides,” *Physical review letters*, vol. 120, no. 1, p. 016401, 2018.
- [7] F. Flicker, F. de Juan, B. Bradlyn, T. Morimoto, M. G. Vergniory, and A. G. Grushin, “Chiral optical response of multifold fermions,” *Physical Review B*, vol. 98, no. 15, p. 155145, 2018.
- [8] F. de Juan, A. G. Grushin, T. Morimoto, and J. E. Moore, “Quantized circular photogalvanic effect in Weyl semimetals,” *Nature communications*, vol. 8, p. 15995, 2017.
- [9] D. S. Sanchez, I. Belopolski, T. A. Cochran, X. Xu, J.-X. Yin, G. Chang, W. Xie, K. Manna, V. Süß, C.-Y. Huang, N. Alidoust, D. Multer, S. S. Zhang, N. Shumiya, X. Wang, G.-Q. Wang, t.-r. Chang, C. Felser, S.-Y. Xu, S. Jia, H. Lin, and M. Z. Hasan, “Topological chiral crystals with helicoid-arc quantum states,” *Nature*, vol. 567, no. 7749, p. 500, 2019.
- [10] N. B. Schröter, D. Pei, M. G. Vergniory, Y. Sun, K. Manna, F. de Juan, J. A. Krieger, V. Süß, M. Schmidt, P. Dudin, B. Bradlyn, T. K. Kim, T. Schmitt, C. Cacho, C. Felser, V. N. Strocov, and Y. Chen, “Chiral topological semimetal with multifold band crossings and long fermi arcs,” *Nature Physics*, p. 1, 2019.
- [11] Z. Rao, H. Li, T. Zhang, S. Tian, C. Li, B. Fu, C. Tang, L. Wang, Z. Li, W. Fan, J. Li, Y. Huang, Z. Liu, Y. Long, C. Fang, H. Weng, Y. Shi, H. Lei, Y. Sun, T. Qian, and H. Ding, “Observation of unconventional chiral fermions with long fermi arcs in *cosi*,” *Nature*, vol. 567, no. 7749, p. 496, 2019.
- [12] D. Takane, Z. Wang, S. Souma, K. Nakayama, T. Nakamura, H. Oinuma, Y. Nakata, H. Iwasawa, C. Cacho, T. Kim, H. Kumigashira, T. Takahashi, Y. Ando, and T. Sato, “Observation of chiral fermions with a large topological charge and associated fermi-arc surface states in *cosi*,” *Physical review letters*, vol. 122, no. 7, p. 076402, 2019.
- [13] N. Schröter, S. Stolz, K. Manna, F. de Juan, M. G. Vergniory, J. A. Krieger, D. Pei, P. Dudin, T. K. Kim, C. Cacho, *et al.*, “Observation and manipulation of maximal chern numbers in the chiral topological semimetal *pdga*,” *arXiv preprint arXiv:1907.08723*, 2019.
- [14] D. Rees, K. Manna, B. Lu, T. Morimoto, H. Borrmann, C. Felser, J. Moore, D. H. Torchinsky, and J. Orenstein, “Quantized photocurrents in the chiral multifold fermion system *rhsi*,” *arXiv preprint arXiv:1902.03230*, 2019.
- [15] W. Kraut and R. von Baltz, “Anomalous bulk photovoltaic effect in ferroelectrics: a quadratic response theory,” *Physical Review B*, vol. 19, no. 3, p. 1548, 1979.
- [16] V. Belinicher and B. Sturman, “The photogalvanic effect in media lacking a center of symmetry,” *Physics-Uspekhi*, vol. 23, no. 3, pp. 199–223, 1980.
- [17] J. Sipe and A. Shkrebtii, “Second-order optical response in semiconductors,” *Physical Review B*, vol. 61, no. 8, p. 5337, 2000.
- [18] I. Sodemann and L. Fu, “Quantum nonlinear hall effect induced by berry curvature dipole in time-reversal invariant materials,” *Physical review letters*, vol. 115, no. 21, p. 216806, 2015.
- [19] Q. Ma, S.-Y. Xu, H. Shen, D. MacNeill, V. Fatemi, T.-R. Chang, A. M. M. Valdivia, S. Wu, Z. Du, C.-H. Hsu, *et al.*, “Observation of the nonlinear Hall effect under time-reversal-symmetric conditions,” *Nature*, vol. 565, no. 7739, p. 337, 2019.
- [20] N. Kristoffel and A. Gulbis, “Some optical properties of a vibronic ferroelectric and the anomalous bulk photovoltaic effect,” *Zeitschrift für Physik B Condensed Matter*, vol. 39, no. 2, pp. 143–149, 1980.
- [21] R. von Baltz and W. Kraut, “Theory of the bulk photovoltaic effect in pure crystals,” *Physical Review B*, vol. 23, no. 10, p. 5590, 1981.
- [22] N. Kristoffel, R. Von Baltz, and D. Hornung, “On the intrinsic bulk photovoltaic effect: performing the sum over intermediate states,” *Zeitschrift für Physik B Condensed Matter*, vol. 47, no. 4, pp. 293–296, 1982.
- [23] H. Presting and R. Von Baltz, “Bulk photovoltaic effect in a ferroelectric crystal a model calculation,” *physica status solidi (b)*, vol. 112, no. 2, pp. 559–564, 1982.
- [24] C. Aversa and J. Sipe, “Nonlinear optical susceptibilities of semiconductors: Results with a length-gauge analysis,” *Physical Review B*, vol. 52, no. 20, p. 14636, 1995.
- [25] K. Yao, B. K. Gan, M. Chen, and S. Shannigrahi, “Large photo-induced voltage in a ferroelectric thin film with in-plane polarization,” *Applied Physics Letters*, vol. 87, no. 21, p. 212906, 2005.
- [26] Q. Ma, S.-Y. Xu, C.-K. Chan, C.-L. Zhang, G. Chang, Y. Lin, W. Xie, T. Palacios, H. Lin, S. Jia, *et al.*, “Direct optical detection of Weyl fermion chirality in a topological semimetal,” *Nature Physics*, vol. 13, no. 9, p. 842, 2017.
- [27] S.-Y. Xu, Q. Ma, H. Shen, V. Fatemi, S. Wu, T.-R. Chang, G. Chang, A. M. M. Valdivia, C.-K. Chan, Q. D. Gibson, *et al.*, “Electrically switchable Berry curvature dipole in the monolayer topological insulator *WTe2*,” *Nature Physics*, vol. 14, no. 9, p. 900, 2018.
- [28] T. Morimoto, M. Nakamura, M. Kawasaki, and N. Nagaosa, “Current-voltage characteristic and shot noise of shift current photovoltaics,” *Physical review letters*, vol. 121, no. 26, p. 267401, 2018.
- [29] Y. Zhang, F. de Juan, A. G. Grushin, C. Felser,

and Y. Sun, “Strong bulk photovoltaic effect in chiral crystal in the visible spectrum,” *arXiv preprint*

arXiv:1908.08878, 2019.